Luminescence enhancement of a self-organised Y 2 O 3 :Eu 3+ thin film-coated porous alumina membrane

Nora Abdellaoui, Antonio Pereira, T. Kandri, E. Drouard, M. Novotny, Bernard Moine, Anne Pillonnet

Luminescence enhancement of self-organised Y_2O_3-Eu^{3+} thin film-coated porous alumina membrane

N. Abdellaoui[1], A. Pereira[1,†], T. Kandri[1], E. Drouard[2], M. Novotny[3], B. Moine[1], A. Pillonnet[1]

[1] *Univ Lyon, Université Claude Bernard Lyon 1, CNRS, Institut Lumière Matière, F-69622, Lyon, France*

[2] *Institut des Nanotechnologies de Lyon - Université de Lyon, UMR 5270 - CNRS, Ecole Centrale de Lyon, 36 avenue Guy de Collongue, F-69134 Ecully cedex, France*

[3] *Institute of Physics of the Czech Academy of Sciences, Na Slovance 2, 182 21 Prague, Czech Republic*

[†] Corresponding author
E-mail: antonio.pereira@univ-lyon1.fr; Tel: +33 472 448 335

Abstract

Y_2O_3:Eu^{3+} thin films were deposited by pulsed laser deposition (PLD) on unordered porous alumina membranes (PAMs). We showed that by adjusting the deposition parameters, self-organisation of Y_2O_3:Eu^{3+} on the PAM occurs, which leads to the formation of a disordered photonic structure with high index contrast. Luminescence measurements showed a strong enhancement of the red emission (up to 12 times) compared to a continuous layer. We demonstrated experimentally and theoretically that such luminescence enhancement is directly correlated to an increase of the absorption efficiency in the UV range.

Keywords

Luminescence enhancement; rare earth; photonic crystal; porous alumina membrane; pulsed lased deposition

Introduction

Thin films based on rare earth ions (RE) are nowadays largely used for both fundamental research and industrial applications. For example, RE-doped thin films are investigated due to their ability to convert light (via down-shifting, down-conversion and up-conversion processes), thus opening a new alternative way to improve the solar cells' efficiency.[1-6] However, due to the low absorption cross-section of the RE ions, the efficiency of the converting layer needs to be increased. Attempts to enhance the rare-earth ions' absorption have led to the development of three main approaches. The first relies on the use of a third rare-earth ion presenting a 4f-5d parity-allowed transition; for example it has been successfully applied to achieve efficient sensitisation of quantum-cutting with the Pr^{3+}-Yb^{3+} couple.[7,8] Another concept combines a rare-earth doped thin layer with plasmonic resonances in the UV and the visible range by using nanostructures made of gold,[9-11] silver[9,10,12,13] or aluminum.[14,15] Another more recently proposed solution is to associate a converting layer with a photonic crystal (PhC) allowing the control of light-matter interaction. Depending on the geometrical parameters of the photonic structure, it is therefore possible to enhance the photon lifetime in the active material, and thus the rare-earth ions' absorption[16] and/or to improve the extraction efficiency of the converting layer.[17,18] The PhC is either patterned directly in the conversion layer, or in a transparent and high refractive index layer deposited on the top of the active layer. In both cases, lithographic fabrication technologies are routinely used. However, this approach requires a complex and a multistep fabrication (i.e. numerous chemical, thermal and etching associated steps), which is time-consuming and not cost-effective.

In this article, we propose an alternative fabrication method of PhC based on the use of unordered porous alumina membranes (PAMs) as a substrate. The use of PAMs was pioneered by Martin's groups, as an evaporation mask for the preparation of nanodot arrays with variable dot size and dot-dot-separation distance.[19] PAMs have attracted much attention owing to the fact that they permit nanofabrication by self-organisation of functional materials with a broad range of potential applications, e.g. electrochemical sensing,[20] as well as optical devices.[21-23] The fabrication of two-dimensional PhC based on porous alumina is well described.[24] Combining the PAM with a layer of high refractive index that mimics the structure of the underlying PAM should lead to a modification of the transmission in the layer of interest, and therefore allow the fabrication of a PhC using a minimal number of processing steps and without the use of expensive lithographical tools. This method is a simple way to

enhance the luminescence quantum efficiencies of the any kind rare earth doped materials. Moreover, PAMs with various pore geometries (e.g., unordered or highly ordered nanohole array) are now commercially available, opening thus the possibility to tune easily and more precisely the properties of the optical active layer. In this study, we report the fabrication and characterisation of a disordered photonic structure based on a luminescent layer, i.e. a Y_2O_3:Eu^{3+} thin film. Taking benefit of the self-organisation of Y_2O_3:Eu^{3+} on the PAM during the deposition, this way is used to produce directly in the luminescent layer a disordered photonic structure with high index contrast. The fluorescent properties of this structure are investigated and compared to those of a continuous film. The reasons affecting the luminescent properties of such structure are discussed using RCWA calculations.

Experimental section

Elaboration of disordered photonic structures

Y_2O_3:Eu^{3+} (5 at.%) was deposited by pulsed laser deposition (PLD) using an ArF excimer laser beam (λ = 193 nm, τ = 17 ns, Coherent CompexPro) operating at 10 Hz. The Y_2O_3:Eu^{3+} target was previously synthesised by solid-state reaction (8 h at 1400°C in air) after grinding and mixing Y_2O_3 (99.99% purity, Alfa Aesar) and Eu_2O_3 (99.999% purity, Alfa Aesar). Thin films were grown at room temperature in an oxygen-gas atmosphere (P_{O2} = 10^{-3} mbar). The laser fluence was kept constant at 2.6 J cm^{-2} and the target-to-substrate distance was set to 6 cm. The deposition was performed on high-purity fused silica glass (Suprasil grade, Heraeus) and commercial 60 µm-thick porous alumina membranes (Anodisc13, Whatman) consisting of array of holes of 200 nm in diameter (PAM_{200}). The number of laser pulses was adjusted to achieve a 60 nm film thickness. The deposition rate was first determined by means of a profilometer (Tencor Alpha Step 100).

Characterisation

After deposition, the samples were analysed by scanning electron microscopy (SEM, Hitachi S800 FEG). The SEM images were analysed using ImageJ software to determine the average pore diameter (*d*), the average interpore distance (*p*) and the porosity (*P*) of Y_2O_3:Eu^{3+} films deposited on PAMs. Luminescence measurements were performed at room temperature using a tunable pulsed laser (τ = 5 ns, Ekspla NT342B) as the excitation source. The fluorescence was collected through an optical fibre (1.1 mm diameter, NA = 0.2) coupled with a Triax190 spectrometer (Jobin Yvon) equipped with a CCD camera. To eliminate directional scattering

effects, and therefore directional enhancement effects, emission was also measured in an integrating sphere (Labsphere). The excitation spectra were performed using a 450 W xenon lamp associated with a monochromator Gemini 180 (Jobin Yvon). All the spectra (emission and excitation) were corrected by the calibrated sensitivity of the experimental setup.

Simulation details

Photonic crystals structures, made of a single pattern periodically repeated in a regular lattice, can give a good overview of the main optical resonances in the structured membrane.[25] Rigorous coupled-wave analysis (RCWA)[26] was thus used to simulate the structure of Y_2O_3:Eu^{3+} deposited on PAMs and to reflect its photonic crystal behaviour in the UV range (200–300 nm). Given the structural geometry, the properties of the material and of the incident light, the simulation permits us to follow the spread of an electromagnetic wave impinging upon a periodic structure, and thus to derive the absorption spectra of the Y_2O_3:Eu^{3+} layer.

Results and Discussion

Morphological and structural characterisations

The morphology of Y_2O_3:Eu^{3+} thin films deposited, keeping the experimental parameters constant and changing the substrate morphology, is shown in Fig. 1. As expected on Suprasil (Fig. 1a), the film is dense and compact with no appearance of porosity. Consistent with this picture, we showed elsewhere that continuous Y_2O_3 films with a roughness of less than 0.1 nm are obtained on SiO_2 when deposition is performed under similar conditions.[15]

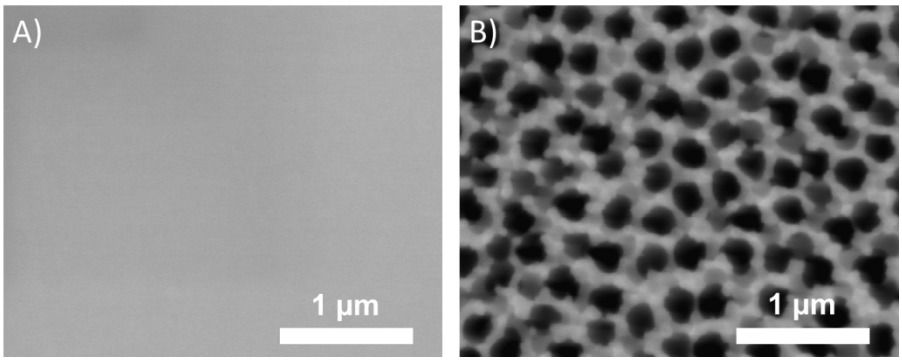

Figure 1 - Top SEM views of Y_2O_3:Eu^{3+} thin films deposited on Suprasil (A) and PAM_{200} (B). The deposition parameters were kept constant, and the equivalent thickness was 60 nm.

For deposition on PAM_{200} (Fig. 1b), the $Y_2O_3:Eu^{3+}$ thin films clearly replicate the porous structure of the underlying substrate, indicating that under these conditions the growth is dominated by the surface diffusion process. This means that the kinetic energy of the species arriving on the surface is high enough to promote diffusion and self-organisation during the deposition. This in in agreement with previous works related to the deposition of metallic (Pt, Au and PtAu)[20] and oxide ($Lu_2O_3:Eu^{3+}$)[23] films on PAM substrates. At high kinetic energies, i.e. under vacuum or moderate background pressure (e.g. $P_{O2} < 10^{-2}$ mbar), the nucleation and growth of particles on the substrate are dominated by surface diffusion processes. Under these conditions, thin or thick macroporous films (up to 300 nm) with pore diameter exceeding 150 nm and replicating the pore structure of the underlying PAM could be prepared. The aspect ratio (*R*) of the PAM substrate, which is defined as the ratio of width to height of the pores, is of about 0.003. With such low value, deposition at the bottom of the pores is therefore excluded. However, deposition inside the pore at depths ranging up to a few hundred of nanometers can be considered. Indeed, previous works[27,28] have demonstrated that it is possible to deposit nanostructures by pulsed laser deposition through a nanostencil having an aspect ratio of about 0.5-0.7. Taking into account this value and considering a pore diameter of 200 nm, it means that $Y_2O_3:Eu^{3+}$ can be theoretically deposited up to about 400 nm in depth. Moreover, A.-L. Thomann et al. have also reported for $R > 0.4$, that the conformity of the films at the side walls is poor (less than 35%).[29] In our case, it means that the film thickness on the pore walls will not exceed 20 nm. The structural parameters of films deposited on PAM_{200} were determined by analysing SEM images and are summarised in Table 1 (more details are given in the supporting information and Fig. SI-1). These values are in fair agreement with the technical data given for the uncovered PAMs.[30] Moreover, according to x-ray diffraction measurements (Fig. SI-2 in the supporting information), $Y_2O_3:Eu^{3+}$ films deposited on Suprasil and PAM_{200} appear amorphous, as no diffraction peaks are observed.

Table 1 - Structural parameters of $Y_2O_3:Eu^{3+}$ films deposited on PAM_{200} determined by analysing SEM images with the ImageJ software.

Pore diameter, *d* (nm)	Period, *p* (nm)	Porosity, *P* (%)
213 ± 28	315 ± 28	52 ± 2

Luminescence properties

Typical emission spectra of a 60 nm-thick Y_2O_3:Eu^{3+} films deposited on Suprasil and on PAM_{200} are displayed in Fig. 2a with a 240 nm excitation wavelength, corresponding to an excitation in the Eu-O charge transfer band (CTB). As described elsewhere in detail,[14] the observed emission peaks are identified as the transitions $^5D_0 \rightarrow {}^7F_J$ (with J = 0–4), and correspond to Eu^{3+} in the cubic phase. These spectra clearly reveal a strong enhancement of the fluorescence properties when the films are deposited on PAM_{200}. Thus between 550–725 nm, the amplification factor goes up to ~12 when Y_2O_3:Eu^{3+} is deposited on PAM_{200}.

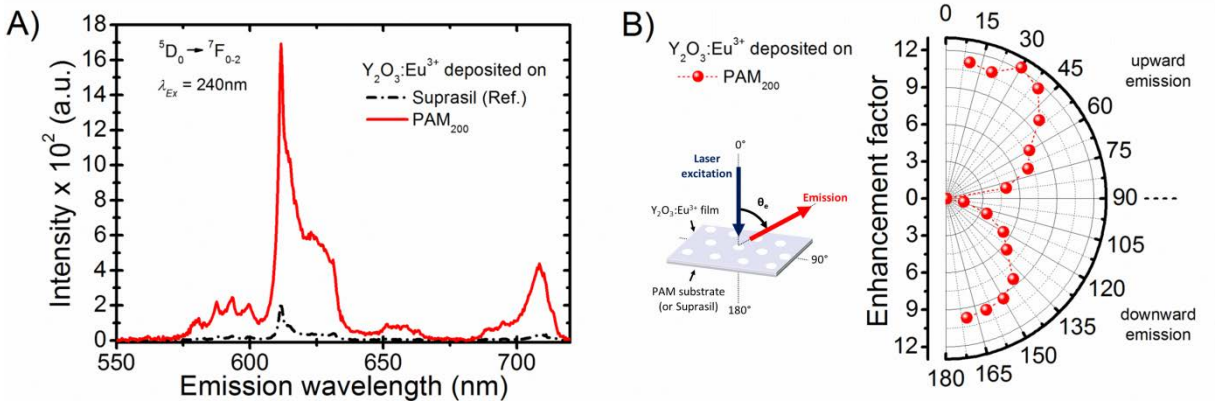

Figure 2 - Luminescence properties of Y_2O_3:Eu^{3+} (60 nm-thick) deposited on Suprasil and PAM_{200} under excitation at 240 nm and at normal incidence: A) typical emission spectra recorded for an emission angle of 30°, B) enhancement factor for Y_2O_3:Eu^{3+} deposited on PAM_{200}.

The angular distribution of emission at 612 nm was also measured for Y_2O_3:Eu^{3+} deposited on PAMs as well as on Suprasil. A sketch of the investigated configuration is shown in the inset of Fig. 2b. By comparison, we determined at different emission angles the luminescence enhancement factor (EF), which is defined as the ratio of the luminescence intensity of Y_2O_3:Eu^{3+} coated on PAMs to that on the Suprasil. Values higher than one indicate a fluorescence enhancement, while those lower than one correspond to a quenching of the luminescence. The distribution of enhancement factor versus emission angle (θ_e) is shown in Fig. 2b, and a strong enhancement of emission up to 12 times is observed. Moreover, even if EF noticeably decreases for angles ranging from 60 to 120°, this structure presents a wide angular distribution for the upward and downward emission. Such angular independence of the enhanced emission is due to the fact that the film structure is non-ordered, and this behaviour differs from the angular dependence of light emission, when 2D photonic crystals are for example used to improve the light extraction.[31] It is worth noting that this behaviour

can be interesting for many applications (e.g lighting, and display), in which a strong variation of the intensity with the emission is undesirable. Comparing now the upward and downward enhancement, it also appears that the upward emission is more pronounced (typically ~58%). In fact, the enhancement of the downward emission is underestimated. Indeed, independent measurements (not described here) have allowed us to estimate that the PAMs absorb ~94% of the light at 612 nm, which suggests a downward emission far higher than the upward one. To investigate the role of the structure orientation with respect to the excitation source, we also measured the emission spectra of Y_2O_3:Eu^{3+} films deposited on PAM_{200} for an incident angle ranging from 0 to 60° and a conic angle of 0°, 45° and 90° (Fig. SI-3 in the supporting information). All these measurements were performed in the integrating sphere in order to obtain the "true" emission intensity, and the recorded signal was corrected by the cosine of the incident angle. At incidence angles up to 60° and whatever the conic angle, the values of the emission intensity remain high and are weakly dependent on the incidence angle as well as on the conic angle. This expected result can be explained by the fact that the film structure is non-ordered and randomly oriented (see Fig. 1b). As a result, the incident angular dependence is averaged, therefore leading to excitation angular-independent emission.

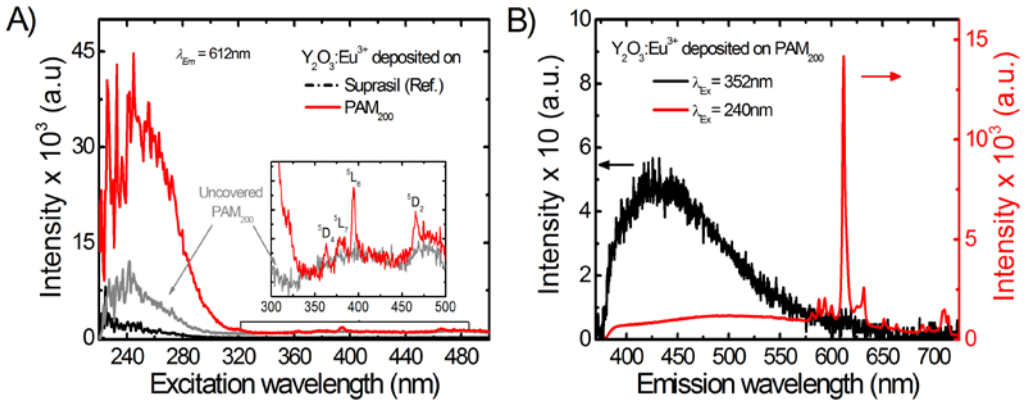

Figure 3 - A) Excitation spectra monitored at 612 nm for Y_2O_3:Eu^{3+} (60 nm-thick) deposited on Suprasil (black curve) and PAM_{200} (red curve). The excitation spectrum of uncovered PAM is also given by the grey curve. The expanded intensity between 300 and 500 nm is shown in the inset with the typical excitation levels of Eu^{3+}. B) Emission spectra for a film deposited on PAM_{200} under excitation at 240 and 352 nm.

As shown in Fig. 3a, such an enhancement is also present in the excitation spectra of the emission of Eu^{3+} at 612 nm. The excitation spectrum of Eu^{3+} shows two patterns: i) one between 200–320 nm that corresponds to the CTB; and ii) another between 350–500 nm, which is assigned to the f-f intra-configurational transitions. After subtraction of signal of the

membrane, we found that the intensity of the CTB at 240 nm is enhanced ~10.5 times on PAM_{200} compared to the reference, which is in agreement with the value obtained for the emission enhancement at 612 nm (~ x 11.5 for integrated intensity at 612 ± 7 nm; see Fig. 2a). Thus, the intensity of excitation band around 240 nm closely follows the intensity of emission at 612 nm, suggesting that no energy transfer process between PAM and Eu^{3+} occurs. In order to point out that the observed enhancement on PAM is due to the Y_2O_3:Eu^{3+} film itself rather than a transfer between the PAM and the luminescent layer (as suggested by Peng et al.[32]), a direct excitation of the membrane at 352 nm, where no direct excitation of Eu^{3+} ions occurs (see inset of Fig. 3a), was performed. As shown in Fig. 3b, the emission spectrum did not show any emission peak at 611 nm, which demonstrates that no energy transfer occurs from the membrane (the excitation and emission spectra of the membrane are given in the supporting information and Fig. SI-4). This measurement confirms the fact that the enhancement of the luminescence properties is due to the self-organisation of the Y_2O_3:Eu^{3+} layer and its structure when deposited on PAMs.

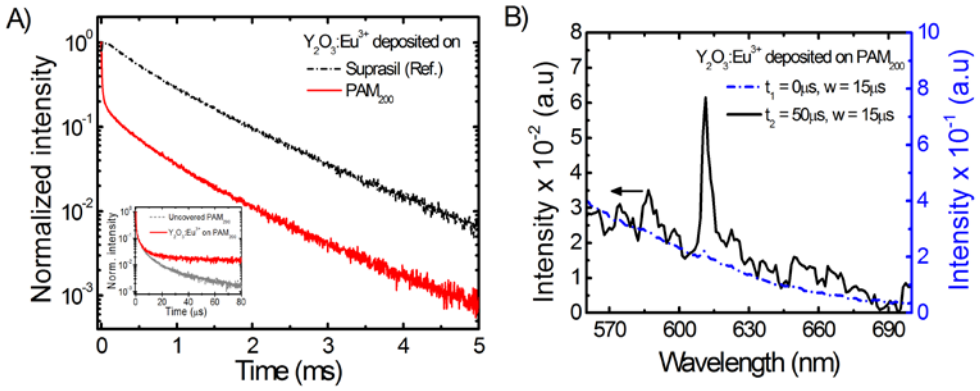

Figure 4 - A) Normalised photoluminescence decay for a 60 nm-thick Y_2O_3:Eu^{3+} film deposited on Suprasil and on PAM_{200} under excitation at 240 nm. The black curve corresponds to the emission of Eu^{3+}, while the red curve corresponds to the mixed emission of the membrane and of Eu^{3+}. In the inset, decays of uncovered membrane and covered membrane are displayed, showing that the fast decay is clearly due to the emission of the membrane. B) Time-resolved photoluminescence for a 60 nm-thick Y_2O_3:Eu^{3+} film deposited on PAM_{200} recorder at two different times.

The observed luminescence enhancement can be explained by an improvement in the absorption efficiency, the extraction efficiency, or a combination of both. As follows from the decay measurements performed at 612 nm for Y_2O_3:Eu^{3+} coated on PAM_{200} and on Suprasil (Fig. 4a), the evolution of the luminescence decays is slightly different. On Suprasil, the decay is exponential and the luminescent lifetime was about 1.1 ms, which corresponds well to the data of Eu^{3+} in the literature.[33] In contrast, on PAM_{200} two decay components can be

clearly distinguished: i) a fast decay time corresponding to the emission of the membrane as shown by the comparison made with uncovered membrane at short time (see inset), and ii) a long decay (~1 ms) that corresponds to the luminescence of Eu^{3+}. These results are supported by the time-resolved photoluminescence measurements performed on the coated membrane. Indeed, Fig. 4b shows that for short delays (t = 0 µs), the emission signal arises only from the membrane, whereas for longer delays (t = 50 µs) a typical emission of Eu^{3+} is obtained with a residual emission from the membrane. Finally, the results presented here show that the luminescent lifetime of Eu^{3+} does not change (1.1 ± 0.1 ms), indicating that the emission enhancement is only related to an increase of the absorption in the UV range, thanks to the structure of the Y_2O_3:Eu^{3+} layer.

Simulation results

To understand the luminescence enhancement, we need to consider light collection and trapping mechanisms allowing an improvement of the absorption in the UV range. First, for an absorbing layer with a non-ordered structuration, it is well known that the light can be efficiently diffracted into various oblique angles to enhance the absorption length compared with an unpatterned layer. Indeed, such an absorbing structure leads to an improvement of the absorption by decreasing the reflection and by multiplying the number of propagation angles inside the layer. However, for high index film of small thicknesses (i.e. $< \lambda/n_f$, where n_f is the film's refractive index) this mechanism is less trivial. In this case, the enhancement of absorption by the factor of $2n_f^2$ as described by Yablonovitch[34] is no more valid, due to the discrete set of resonances in the film. We assumed that the Y_2O_3:Eu^{3+} layer deposited on PAMs acts like a disordered photonic structure. To overcome this limitation and to estimate the light collection and trapping performance of our structure, the absorption of the porous Y_2O_3:Eu^{3+} layer deposited on PAM_{200} was calculated in the UV range using the RCWA method (Fig. 5). The parameters used in the simulation to calculate the absorption were the pore diameter (d ± 20 nm), the period (p ± 20 nm), the incidence angle (θ_i = 40°), the azimuthal angle (φ_i = 0°), the polarisation state (TE) and the refractive indices of PAM_{200} ($n_{Al_2O_3}$) and of the porous Y_2O_3:Eu^{3+} layer ($n_{Y_2O_3}$). Here, the structure was modelled using a periodic triangular pattern according to Masuda et al.[35], which is a rough approximation of the real structure. To approach the real structure, the d and p values determined from the SEM image analysis were used, whereas the refractive indices were derived from the literature ($n_{Y_2O_3} = 2.17$[36] and $n_{Al_2O_3} = 1.85$[37] at 240 nm). For calculation, the absorption of Eu^{3+} was

also taken into account by fixing the extinction coefficient of Y_2O_3:Eu^{3+} at 10^{-6}. The height (*h*) of the structure was equal to the Y_2O_3:Eu^{3+} film thickness (i.e. 60 nm); the PAM_{200} thickness was 60 µm. Fig. 5a shows the absorption intensity of the porous Y_2O_3:Eu^{3+} layer deposited on PAM_{200} for various periods. Among many small peaks attributed to Fabry Perot-like modes in the low index PAM_{200} buffer layer, high-intensity resonance peaks appear in this range, indicating an increased absorption in the Y_2O_3:Eu^{3+} layer at specific wavelengths. This can be attributed to an efficient coupling of the impinging light into a pseudo guided mode of the high index film. Their positions and intensity clearly depend on the period of the structure. More precisely, the wavelength λ of the resonances occurring at given normalised frequency λ/p related to the stack and pore diameter *d*, logically increases with the period (clearly visible for two modes and for periods of 310 and 340 nm in Fig. 5a).

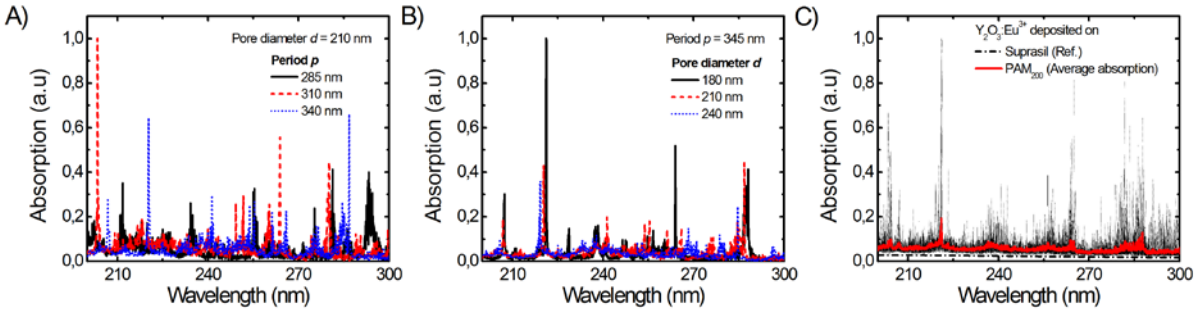

Figure 5 - Simulated absorption spectra for 60 nm-thick layer of Y_2O_3:Eu^{3+} deposited on PAM_{200} using a triangular cell structure: A) changes in absorption spectra depending on the period *p*, B) changes in absorption spectra depending on the pore diameter *d*, and C) global absorption spectrum taking into account the variation of the period and the pore diameter (p = 315 ± 30 nm and d = 213 ± 28 nm, respectively). The red curve corresponds to the average absorption. The simulated absorption spectrum of a Y_2O_3:Eu^{3+} layer on Suprasil is also given (black dashed line).

The same behaviour is observed in Fig. 5b, when the pore diameter is changed, while the period remains constant. Roughly speaking, small holes limit the coupling of the guided waves inside the membrane and the radiative waves; this can justify the highest intensity of the peaks for the smallest diameter, e.g. at ~220 nm. Even if the absorption of light is a wavelength-selective process that relies on the structure order, here we need to take into account the fact that the period as well as the diameter in the real structure is not constant. Thus, to approach further the real porous structure that is disordered, we made the summation of all absorption spectra with *p* and *d* ranging from 285–345 nm and from 185–240 nm, respectively, and calculated an average absorption (Fig. 5c), under the hypothesis of a short coherence length. The absorption enhancement occurs at a larger number of wavelengths but

with a smaller magnitude, as established for pseudo-disordered or correlated disordered structures.[38] Even if the Y_2O_3:Eu^{3+} layer cannot be considered as a perfectly ordered photonic crystal, this result is in agreement with the experimental measurements: the luminescence enhancement of the self-organised Y_2O_3:Eu^{3+} is directly correlated to an increase of its absorption.

Conclusions

In conclusion, we have demonstrated that the luminescence properties of an emitting layer such as Y_2O_3:Eu^{3+} can be significantly improved when deposited on porous alumina membranes. By taking advantage of the self-organisation of Y_2O_3:Eu^{3+} on the PAM during the deposition and of its structure, the emission of the Eu^{3+} ions can be increased by a factor of up to ~12. We have shown that observed luminescence enhancement can be explained by an improvement in the absorption efficiency in the UV range.

Acknowledgements

We thank Dr. Regis Orobtchouk for the RCWA code. The SEM images were taken at the *Centre Technologiques des Microstructures* platform (Faculté des Sciences et Technologies de l'Université Lyon 1). This work was supported by the French Ministry of National Education and Ministry of Higher Education and Research through the Hubert Curien Partnerships (PHC) and the Barrande project 31283ZL / 7AMB14FR010, by the Czech Ministry of Education, Youth and Sports project LO1409 and Czech Science Foundation project 16-22092S.

References

1 B.M. van der Ende, L. Aarts, A. Meijerink, Phys. Chem. Chem. Phys. 11, **2009**, 11081–11095.
2 B.M. van der Ende, L. Aarts, A. Meijerink, Adv. Mater. 21, **2009**, 3073–3077.
3 Q.Y. Zhang, X.Y. Huang, Prog. Mater. Sci. 55, **2010**, 353–427.
4 X. Huang, S. Han, W. Huang, X. Liu, Chem. Soc. Rev. 42, **2013**, 173–201.
5 J.C. Goldschmidt, S. Fischer, Adv. Optical Mater 3, **2015**, 510–535.
6 S.F.H. Correia, V. de Zea Bermudez, S.J.L. Ribeiro, P.S. André, R.A.S. Ferreira, L. Carlos, J. Mater. Chem. A 2, **2014**, 5580–5596.
7 A. Guille, A. Pereira, A. Bensalah-Ledoux, B. Moine, M. Novotny, J. Bulir, P. Fitl, J. Lancok, J. Appl. Phys., 114, **2013**, 203509.

[8] A. Guille, A. Pereira, G. Breton, A. Bensalah-Ledoux, B. Moine, J. Appl. Phys. 111, **2012**, 043104.
[9] M. Eichelbaum, K. Rademann, Adv. Funct. Mater. 19, **2009**, 2045–2052.
[10] S. Derom, A. Berthelot, A. Pillonnet, O. Benamara, A.-M. Jurdyc, C. Girard, G. Colas des Francs, Nanotechnology 24, **2013**, 495704.
[11] S. Fischer, F. Hallermann, T. Eichelkraut, G. von Plessen, K.W. Krämer, D. Biner, H. Steinkemper, M. Hermle, J.C. Goldschmidt, Opt. Express 21, **2013**, 10606–10611.
[12] O.L. Malta, M.A. Couto Dos Santos, Chem. Phys. Lett. 174, **1990**, 13–18.
[13] A. Pillonnet, A. Berthelot, A. Pereira, O. Benamara, S. Derom, G. Colas des Francs, A.-M. Jurdyc, Appl. Phys. Lett. 100, **2012**, 153115.
[14] N. Abdellaoui, A. Pereira, A. Berthelot, B. Moine, A. Pillonnet, Nanotechnology 26, **2015**, 095701.
[15] N. Abdellaoui, A. Pillonnet, B. Moine, J. Penuelas, E. Kovacevic, J. Berndt, A. Pereira, Nanotechnology 26, **2015**, 115604.
[16] T. Deschamps, A. Guille, E. Drouard, R. Mazurczyk, R. Orobtchouk, C. Jamois, A. Fave, R. Peretti, E. Fourmond, A. Pereira, B. Moine, C. Seassal, Proc. SPIE 8620, **2013**, 86200G.
[17] K.-Y. Ko, Y.K. Lee, Y.R. Do, Y.-D. Huh, J. Appl. Phys. 102, **2007**, 013509.
[18] K.-Y. Ko, E.-J Her, W.T. Nichols, H. Lee, Y.R. Do, J. Ahn, Microelectron. Eng. 88, **2011**, 2930–2933.
[19] C.R. Martin, Science 266, **1994**, 1961–1966.
[20] A. Pereira, F. Laplante, M. Chaker, D. Guay, Adv. Func. Mater. 17, **2007**, 443–450.
[21] K.Y. Peng, Y.L. Ho, X.J. Yu, H.S. Kwok, J. Appl. Phys. 96, **2004**, 1649.
[22] A. Santos, T. Kumeria, D. Losic, Materials 7, **2014**, 4297–4320.
[23] A. Pereira, T. Martin, M. Levinta, C. Dujardin, J. Mater. Chem. C 3, **2015**, 4954.
[24] X. Sheng, J. Liu, N. Coronel, A.M. Agarwal, J. Michel, L.C. Kimerling, IEEE Photon. Technol. Lett. 22, **2010**, 1394–1396.
[25] R. Peretti, G. Gomard, L. Lalouat, C. Seassal, E. Drouard, Phys. Rev. A 88, **2013**, 053835.
[26] M. G. Moharam, T. K. Gaylord, J. Opt. Soc. Am. 71, **1981**, 811–818.
[27] F. Vroegindeweij, E.A. Speets, J.A.J Steen, J. Brugger, D.H.A. Blank, Appl. Phys. A 79, **2004**, 743-745.
[28] C.-V. Cojocaru, R. Nechache, C. Harnagea, A. Pignolet, F. Rosei, Appl. Surf. Sci. 256, **2010**, 4777-4783.
[29] A.-L. Thomann, C. Vahlas, L. Aloui, D. Samelor, A. Caillard, N. Shaharil, R. Blanc, E. Millon, Chem. Vap. Deposition 17, **2011**, 366-374.
[30] SPI SUPPLIES, http://www.2spi.com/category/anopore-membranes/filtration/ (last accessed: 26 June 2016).
[31] J.R. Oh, Y.K. Lee, H.K. Park, Y.R. Do, J. Appl. Phys. 105, **2009**, 043103.
[32] A. Peng, E. Xie, C. Jia, R. Jiang, H. Lin, Mater. Lett. 59, **2005**, 3866–3869.
[33] A. Pillonnet, J. Lancok, C. Martinet, O. Marty, J. Bellessa, C. Garapon, J. Phys.: Condens. Matter 18, **2006**, 10043–10058.
[34] E. Yablonovitch, J. Opt. Soc. Am. 72, **1982**, 899.
[35] H. Masuda, M. Ohya, H. Asoh, M. Nakao, M. Nohtomi, T. Tamamura, Jap. J. Appl. Phys., 38, **1999**, L1403.
[36] Refractive index database, http://refractiveindex.info/ (last accessed: 26 June 2016).

[37] D. Losic, A. Santos in Nanoporous Alumina - Fabrication, Structure, Properties and Applications (Springer, New York, 2015).
[38] K. Vynck, M. Burresi, F. Riboli, D. Wiersma, Nat. Mater. 11, **2012**, 1017–1022.